# Influence of Precursor Structure on the Properties of Polyacrylonitrile-Based Activated Carbon Hollow Fiber

MING-CHIEN YANG* and DA-GUANG YU

Department of Textile Engineering, National Taiwan Institute of Technology, 43, Keelung road, Section 4, Taipei, Taiwan 10672, Republic of China

SYNOPSIS

Three types of precursors of polyacrylonitrile (PAN) hollow fibers were used to produce activated carbon hollow fibers (ACHF). These precursors are different in the structure and composition. Characterization were performed including tensile strength, modulus, x-ray diffraction, pore size distribution, and surface area measurement for the resulting ACHF. The results show that the ACHF produced from the precursor with larger crystal size and dense structure has higher mechanical properties, whereas the ACHF from the precursor with smaller crystal size and porous structure has larger surface area and broader pore size distribution. © 1996 John Wiley & Sons, Inc.

## INTRODUCTION

Asymmetric membranes were developed in the 1950s. These membranes have a very thin, dense skin on one surface, supported by a porous substructure.[1] The structure of hollow fiber membranes depends on the material as well as the method of preparation. It is possible to predict the pore size distribution from the polymer solution thermodynamics and phase separation. The inherent advantage of favorable membrane surface area to total separator volume is a well-established principle for the hollow fiber systems.[2] Typical hollow fibers are self-supporting tubes with inside diameters ranging form 0.04 to 2 mm. The process operating pressure limits the fiber size.[1] The main purpose of this support is to eliminate substantial substructure resistance of gas transport and to provide hollow fibers with reasonable mechanical properties such as compressive strength and collapse pressure.[3] Commonly used polymers for making hollow fiber include cellulose acetates, regenerated cellulose, polyamides, polysulfones, and blends of polyvinyl chloride (PVC), polyacrylonitrile (PAN).[1]

Polyacrylonitrile fibers are of great importance both in the textile industry and for marking high-quality carbon fibers.[4] Many researchers have reported the development of carbon fibers with PAN as the precursor material.[5] Pyrolysis of PAN fibers in the oxidation process is necessary to develop the carbonized fibers and activated carbon fibers. The first stage, the oxidation process of the PAN fiber, is best achieved in air between 200 and 300°C. It will convert the precursor to an infusible stable ladder polymer for subsequent higher temperature processing. Carbonization, the second stage, in an inert atmosphere (pure nitrogen) at 1000–2000°C, will increase the carbon content. The carbon fibers produced in this temperature range are then activated at 800~1000°C in carbon dioxide. Activated carbon fiber (ACF) is a highly efficient adsorbent that has a considerable geometric surface and has a number of new applications.[6-9] Koresh and Soffer groups recently obtained a patent covering the making of carbon membranes though controlled pyrolysis to produce carbon hollow fiber for gas separation and showed high fluxes and good selectivities.[10,11] Schindler and Maier[12] obtained another patent for making hollow carbon fiber membrane, in which the PAN hollow fiber was pretreated with hydrazine and then followed by oxidation and carbonization, and is suitable for separating particles. Yoneyama and Nishihara have obtained a patent on the carbonized PAN hollow fiber.[13] Linkov et al. have carbonized the PAN hollow fiber and examined the surface

* To whom correspondence should be addressed.

Journal of Applied Polymer Science, Vol. 59, 1725–1731 (1996)
© 1996 John Wiley & Sons, Inc. CCC 0021-8995/96/111725-07

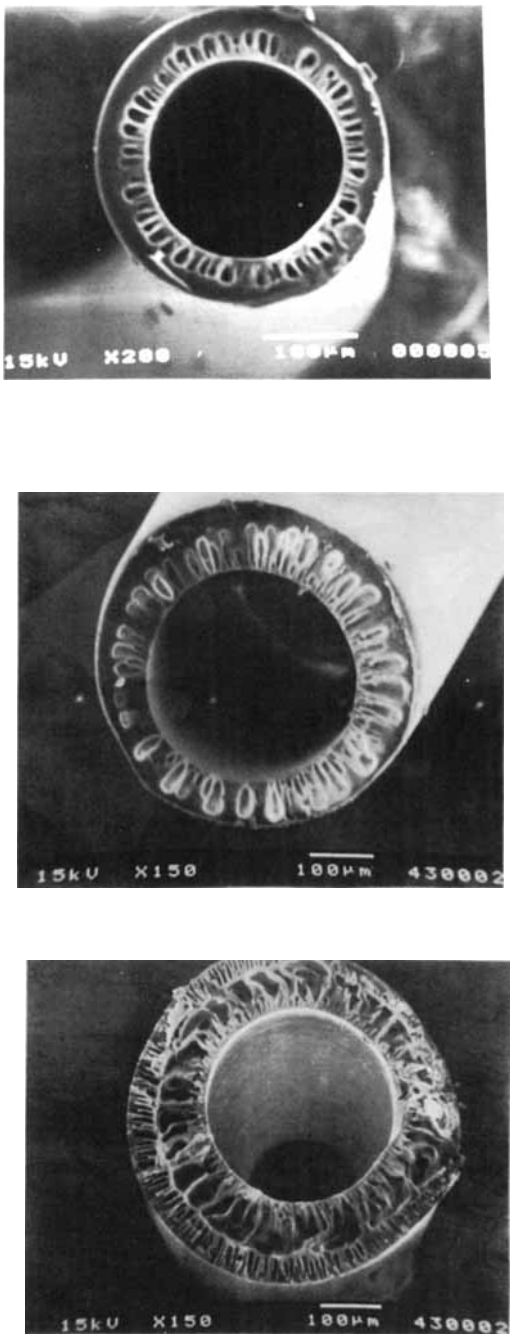


(a)

(b)

(c)

**Figure 1** SEM micrographs of the cross-section of various hollow PAN fibers: (a) sample A (b) sample B, and (c) sample C.

structure of the resulting hollow fibers with scanning probe microscopy (SPM).[14] However, because the carbon material is known to have a high affinity for bacteria,[15] ACHF with much higher membrane area per unit volume is generally superior to original membrane in thermal, mechanical, and structure stability, chemical and microbiological resistance, and ease of cleaning and regenerating. Activated carbon hollow fibers have an adsorptive capability of activated carbon, and we may control the size and distribution of the pores by temperature and time duration.

In this work, three types of hollow fiber precursors with different compositions and porous structure were oxidized, carbonized, and activated under the same conditions. Their properties such as strength, modulus, crystal size, morphology, surface area, and pore size distribution were compared and discussed. The results are helpful for understanding the influence of the structure of the precursor on the characteristics of the resulting activated carbon hollow fiber.

## EXPERIMENTAL

### Preparation of Precursor Samples

One of the three samples, sample A, was obtained from a dialyzer (Asahi PAN-85). Samples B and C were prepared in this laboratory. The procedures were mentioned in our previous article.[16] The average molecular weight and polydispersity of PAN were determined using a gel permeation chromatographer (Model 440, Waters Associates). The mobile phase was *N,N*-dimethyl formamide (DMF) containing 0.5 wt % of LiBr, and the GPC column used was $\mu$-Bondagel E-Linear (Waters Associates).

### Preparation of Activated Carbon Hollow Fiber

The PAN hollow fiber was first oxidized in air at 230°C for 5 h. The oxidized hollow fiber was then heated in nitrogen at 1000°C for 40 min to form the carbon hollow fibers. Final activation was carried out at 800°C for 40 min in the presence of carbon dioxide.

### Characterization of Activated Carbon Hollow Fiber

The mechanical properties of the hollow fibers and the activated carbon hollow fibers were determined using a tensile testers (Vibroskop, Lenzing AG) with a testing speed of 1 mm/min and a testing gauge of 10 mm. In each case, about 25 specimens were tested and the averages were taken. The crystal size of the fiber was determined by an x-ray diffractometer (Seintage DMS 2000) using Ni-filtered Cu$K_\alpha$ radiation. The crystal size (*Lc*) was estimated by the Scherrer equation[17]

**Table I The Chemical Compositions and Properties of Precursor PAN Hollow Fiber**

| Sample | $\bar{M}_w$ | $\bar{M}_w/\bar{M}_n$ | Elemental Analysis N% | C% | H% | Lc (nm) | Tensile Strength (GPa) | Modulus (GPa) |
|---|---|---|---|---|---|---|---|---|
| A | 326,000 | 1.9 | 25.67 | 66.71 | 5.57 | 2.51 | 0.80 | 47 |
| B | 307,000 | 2.0 | 20.13 | 60.51 | 6.47 | 1.29 | 0.60 | 21 |
| C | 307,000 | 2.0 | 20.13 | 60.51 | 6.47 | 0.88 | 0.47 | 16 |

$$Lc = \frac{k\lambda}{B\cos\theta}$$

where $\lambda$ is the wavelength of $CuK_\alpha$ x-ray, $B$ is the width at half-maximum intensity of the peak at $2\theta = 17°$ for PAN fiber and 26° for activated carbon fiber, respectively, and the factor $k$ is 0.89. The aromatic index ($AI$) was determined according to the following formula:[18]

$$AI(\%) = \frac{I_a}{I_a + I_p}$$

where $I_a$ is the diffraction pattern given by the ladder polymer at $2\theta = 26°$, and $I_p$ is the diffraction by the PAN crystal at $2\theta = 17°$. A scanning electron microscope (SEM) (Cambridge S-360) was used to examine the cross-section and the surface of the fiber. The surface area of the ACHF was determined by nitrogen adsorption at 77 K after degassing at pressure below $10^{-3}$ Torr for 12 h using a BET porosimeter (Quantachrome Autosorb-6). The pore size distribution of the ACHF was determined using a mercury intrusion porosimeter (Quantachrome Autosorb-60) under the pressure ranged from 0 to 400 MPa. The compositions of the fibers were determined using an elemental analyzer (Heraeus CHN-O-RAPIO).

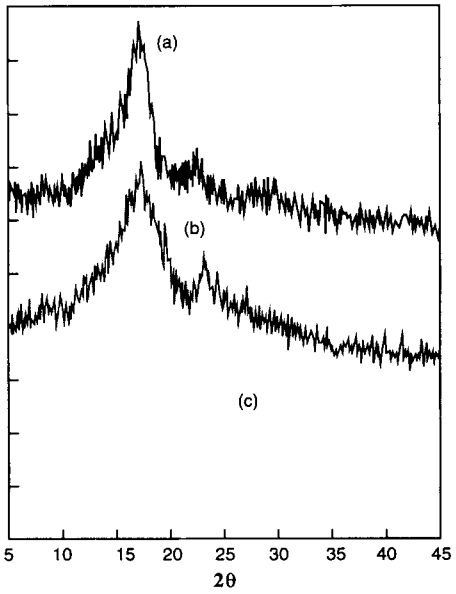


**Figure 2** Wide-angle x-ray diffractograms of hollow PAN fibers: (a) sample A (b) sample B, and (c) sample C.

## RESULTS AND DISCUSSION

### Structure and Properties of Precursor PAN Hollow Fiber

Generally, the dope for making hollow fiber is composed of polymer, solvent, and additive. Cabasso et al.[19-21] have discussed the relationship between the dope composition and the structure of hollow fiber. Because homopoly-acrylonitrile is not easily dissolvable and has a high cyclization temperature during oxidation, the introduction of a few percent of comonomer into polymer chains can improve these disadvantages.[22-33] Shown in Figure 1 are the SEM micrographs of the porous structure of these three samples. Samples A and B have similar finger-like structure, and sample C has dual-layer porous structure. However, samples B and C were of the same chemical composition. The difference in the structure was due to the dope composition. Sample B was prepared from a 20% dope, while sample C was from a 10% dope.

Table I shows the molecular weights, polydispersities, compositions, and mechanical properties

**Table II The Properties of Oxidized Hollow Fibers**

| Sample | AI (%) | Tensile Strength (GPa) | Modulus (GPa) | Elongation (%) |
|---|---|---|---|---|
| A | 51.8 | 0.68 | 23.1 | 6.04 |
| B | 54.3 | 0.52 | 16.9 | 4.01 |
| C | 60.2 | 0.41 | 6.3 | 2.89 |

**Table III The Properties of Carbon Hollow Fibers**

| Sample | Lc (nm) | Tensile Strength (GPa) | Modulus (GPa) | Elongation (%) |
|---|---|---|---|---|
| A | 1.42 | 1.55 | 79.3 | 2.16 |
| B | 1.02 | 1.11 | 66.8 | 1.75 |
| C | 0.90 | 0.56 | 31.2 | 1.03 |

of the precursor PAN hollow fibers used in this work. These samples have similar molecular weights. The molecular weight of sample A is 32,7000, and those of samples B and C are 306,000. The polydispersities of these samples are about the same: 1.9 for sample A, and 2.0 for samples B and C. Sample A with more acrylonitrile units (high nitrogen content) has the largest crystal size (*Lc*) of 2.51 nm, as shown in Figure 2 and Table I. Samples B and C have the crystal size of 1.29 and 0.81 nm, respectively, due to their lower acrylonitrile content. Because sample A has less and smaller pores and larger crystal size, its tensile strength and modulus was higher. Because of smaller crystal size and lower acrylonitrile content, sample B has lower tensile strength and modulus, although its structure is similar to sample A. Because of the dual-layer structure, sample C has the smallest crystal size and the lowest tensile strength and modulus.

## Structure and Properties of Oxidized PAN Hollow Fibers

When the PAN fiber was heated, ladder-polymer began to form above 200°C.[34] Because both inner and outer surfaces of the hollow fiber were attacked by oxygen, the morphology of oxidized hollow fibers (OHF) is different from oxidized solid fibers. Dense ladder structure was formed in the skin region of the wall of OHF, whereas the original microvoid and finger-like structure was driven toward the inner region of the wall.

As show in Table II, sample A has the highest tensile strength and modulus. This is because sample A has the largest crystal size (see Table I), thus makes it less susceptible to the attack of oxygen and, hence, causes less chain scission during oxidation. In addition, because the acrylonitrile content of sample A is higher, its cyclization was more complete, and the ladder-structure was more perfect. On the other hand, with lower acrylonitrile content, the stacking in the ladder-structure for samples B and C is, thus, inferior to sample A, and leads to lower mechanical strength of the resulted OHF. In particular, the permeation of oxygen is much easier in its porous structure, sample C thus has the highest *AI* value.

## Structure and Properties of Carbonized Hollow Fibers

During carbonization, hollow fibers with higher acrylonitrile content are less likely to lose its low molecular weight matters. These low molecular weight matters resulted from the thermal degradation of those structure not involved in the cyclization reaction in the oxidation stage. As shown in Tables I and III, the strength of sample A was stronger than sample B by 33% before oxidation, and by 40% after carbonization. Similarly, the difference between samples B and C was 27% before oxidation and 73% after carbonization. This suggests that the amorphous region and porous structure became brittle after carbonization, thus enlarging the difference in the strength. After carbonizing at 800°C, denitrogenation occurred and the network structure formed. The fiber becomes more dense, and smaller in diameter.[35] For sample A, with high crystallinity, graphitoidal structure resulted at 1000°C in nitrogen during carbonization. This caused the internal region of the fiber to condense, namely, a reduction in the number of pores that was concentrated in the center of the wall of the hollow fiber. As for samples B and C, with lower acrylonitrile content and lower crystallinity, the stacking of the ladder-structure became less orderly from the originally more irregular manner during oxidation. During carbonization, thermal degradation of this irregular structure became pits and pores on the surface of samples B and C. Balasubramanian et al.[36] reported that the open pores are converted to closed pores in the process of carbonization. However, the number of micropores will increase gradually at carbonization temperature above 1000°C. Therefore, for the most porous sample C, its pores became larger, the wall became thinner, and micropores formed.

## Structure and Properties of Activated Hollow Fibers

The activation mechanism of the activated gas and the carbon structure is essential to the development of pores. Marsh et al.[37] suggested that the coarseness just begins at the brim or defective sites of the crystal. The cracks of such a graphitoidal structure are deprived by $CO_2$ and evolved into pores. In the case of this activation, the disorganized carbons are first

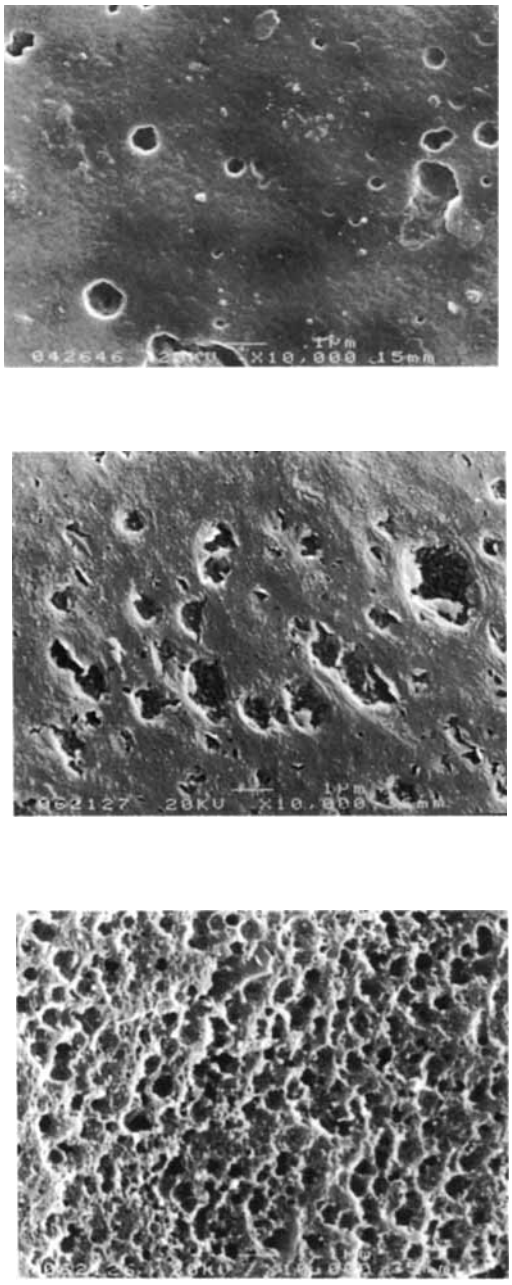

**Figure 3** SEM micrograph of the surface of activated hollow carbon fibers: (a) sample A (b) sample B, and (c) sample C.

activated, causing the opening of the closed pores. Afterwards, the nongraphitoidal carbonic atoms and partial graphitic carbons on the exterior of the activated carbon hollow fiber are gasified, bringing about broader pores and exhibiting the draped and etched (degraded) morphology, as shown in Figure 3. The properties of the ACHF activated from the carbon hollow fiber are shown in Table IV. The crystalline size ($Lc$) of ACHF is usually smaller than

**Table IV The Properties of Activated Carbon Hollow Fibers**

| Sample | Lc (nm) | Tensile Strength (GPa) | Modulus (GPa) | Elongation (%) | Yield (%) |
|---|---|---|---|---|---|
| A | 1.42 | 1.51 | 80.1 | 1.02 | 67 |
| B | 0.96 | 0.92 | 67.2 | 0.83 | 46 |
| C | 0.81 | 0.32 | 30.4 | 0.67 | 40 |

that of the precursor PAN hollow fiber, and increases with the carbonization temperature.[34]

As shown in Table IV, the tensile strength and modulus of the activated samples are better than their PAN precursors. As far as the mechanical properties are concerned, the higher the mechanical properties of the hollow PAN fiber are, the higher the mechanical properties of the activated hollow fiber. The scission of the molecular chain in the oxidation process and the evolution of the low molecular weight matters in the carbonization process lead to the reaction of carbon element with carbon dioxide to produce carbon monoxide.[38] The evolving of CO causes the loss of weight in the fibers. Therefore, after sustained the attack of $CO_2$, the coarseness of the sample A gradually increased. As shown in Figure 3, samples A and B have less porosity than sample C. This is because dehydrogenation and deni-

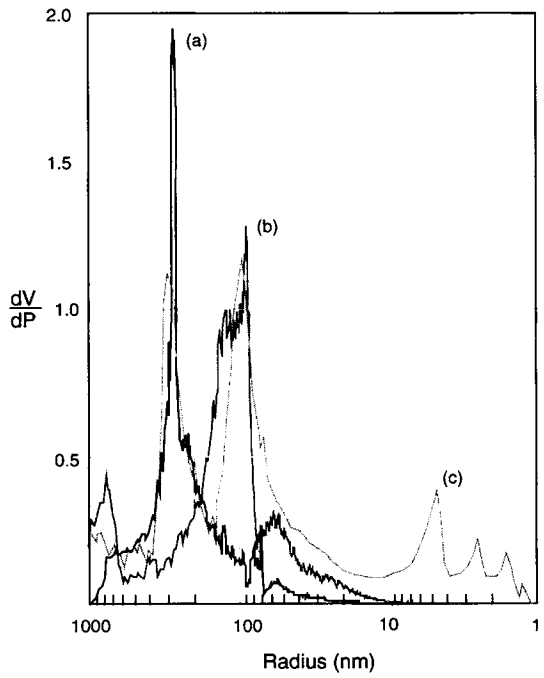


**Figure 4** The pore size distribution of activated hollow carbon fibers: (a) sample A (b) sample B, and (c) sample C.

trogenation during carbonization in sample C caused more gas volatilization and increased the porosity in the interior of ACHF; thus, its fiber properties after activation were inferior to those of samples A and B. Also shown in Table IV, the carbon yield of sample A is higher. This is because sample A has higher acrylonitrile content, which results in better crystallization and less gas volatilization during carbonization and activation. There is a considerable reduction of carbon yield in sample C. This suggests that the hollow PAN fiber with inferior crystallization is more susceptible to chain scission at the oxidation stage. Therefore, sample C has the lowest mechanical properties among these three samples.

### Pore Size Distribution and Surface Area of Activated Carbon Hollow Fibers

The pore size distribution of ACHF was determined with the mercury intrusion method (MIP). As shown in Figure 4, sample A has a larger peak at 300 nm, sample B has a larger peak at 100 nm, and sample C has two larger peaks at 300 and 100 nm, with three smaller peaks located between 10 to 1 nm. This is because the skin structure of sample C is thinner, and larger pores can be more easily created by the etching of $CO_2$. In addition, during activation, $CO_2$ etched the carbon planes, thus promoting the degradation of the structures and creating new pores on the fiber surface; hence, widened the distribution.

The surface area of ACHF was determined with the nitrogen adsorption method. As shown in Figure 5 and Table V, sample C shows the largest hysteresis in the adsorption–desorption curve; thus, it has the largest surface area than those of samples A and B. This is because sample C has more pores on the surface of the fiber (see Fig. 3) and more chain scission in the amorphous phase. Although sample C has lower mechanical properties and carbon yield than samples A and B, it has more pores, wider pore size distribution, and larger surface area. In other words, sample C has better activation characteristics than samples A and B.

**Table V The Composition and Surface Area of Activated Carbon Hollow Fibers**

| Sample | Elemental Analysis N% | C% | H% | O% | Surface Area ($m^2/g$) |
|---|---|---|---|---|---|
| A | 11.78 | 81.06 | 0.78 | 4.6 | 283 |
| B | 11.43 | 80.62 | 0.75 | 5.28 | 307 |
| C | 11.09 | 79.38 | 0.71 | 6.71 | 340 |

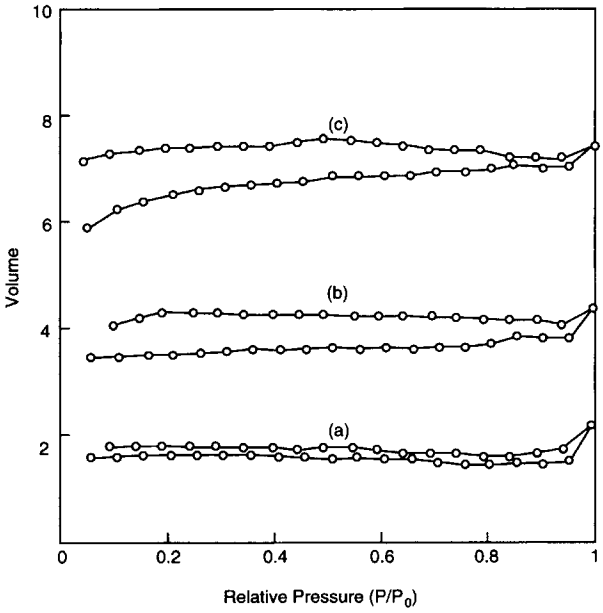


**Figure 5** The nitrogen sorption isotherms of activated carbon hollow fibers: (a) sample A (b) sample B, and (c) sample C.

## CONCLUSION

For a precursor with higher acrylonitrile content and dense structure, the crystal size ($Lc$), tensile strength, and modulus are higher. During oxidation, such a precursor is less susceptible to the attack of oxygen. This causes the resulted activated carbon hollow fiber to have higher mechanical properties, narrower pore size distribution, and lower surface area. On the other hand, a precursor with very porous structure and smaller crystal size is more susceptible to the attack of oxygen and carbon dioxide. The resulted ACHF has lower mechanical properties, wider pore size distribution, and larger surface area. Thus, to meet the requirement of the application, a suitable activated carbon hollow fiber can be prepared from a precursor with the proper structure.

## REFERENCES

1. J. I. Kroschwitz (Ed.), *Encyclopedia of Polymer Science and Engineering*, 2nd ed., Vol. 17, Wiley Interscience, New York, 1985, pp. 76–93.
2. R. Mckinney, Jr., *Desalination*, **62**, 37 (1987).
3. T.-S. Chung, E. R. Kafchinski, R. S. Kohn, P. Foley, and R. S. Straff, *J. Appl. Polym. Sci.*, **53**, 701 (1994).
4. O. P. Bahl, R. B. Mathor, and K. D. Kundra, *Fiber Sci. Technol.*, **15**, 147 (1981).

5. O. P. Bahl and L. M. Manocha, *Carbon,* **12,** 417 (1974).
6. S. F. Grebennikov and L. I. Fridman, *Fiber Chem.,* **19,** 385 (1987).
7. M. Kuroda, M. Yuzawa, Y. Sakakibara, and M. Okamura, *Water Res.,* **22,** 653 (1988).
8. M. Suzuki, *Carbon,* **32,** 577 (1994).
9. I. Mochida, T. Hirayama, S. Kisamori, S. Kawano, and H. Fujitsu, *Langmuir,* **8,** 2290 (1992).
10. J. E. Koresh and A.Soffer, *Sep. Sci. Technol.,* **18,** 723 (1983).
11. A. Soffer, J. E. Koresh, and S. Saggy, U.S. Pat. 4,685,940 (1987).
12. E. Schindler and F. Maier, U.S. Pat. 4,919,860 (1990).
13. H. Yoneyama and Y. Nishihara, U.S. Pat. 5,089,135 (1991).
14. V. Linkov, R. D. Sanderson, and E. P. Jacobs, *J. Mater. Sci. Lett.,* **13,** 600 (1994).
15. A. Oya and S. Yoshida, *Carbon,* **31,** 71 (1993).
16. M.-C. Yang and D.-G. Yu, *J. Appl. Polym. Sci.,* to appear.
17. B. D. Cullity, *Element of X-Ray Diffraction,* Addison-Wesley, Reading, MA, 1978.
18. T. Uchida, I. Shiniyama, Y. Ito, and K. Nukuda, Proc. 10th Biennial Conf. on Carbon, Bethlehem, PA, 1971, p. 31
19. I. Cabasso, E. Klein, and E. J. K. Smith, *J. Appl. Polym. Sci.,* **20,** 2377 (1976).
20. I. Cabasso, E. Klein, and E. J. K. Smith, *J. Appl. Polym. Sci.,* **21,** 165 (1977).
21. I. Cabasso, E. Klein, and E. J. K. Smith, *J. Appl. Polym. Sci.,* **20,** 1883 (1977).
22. W. H. Howard, *J. Appl. Polym. Sci.,* **15,** 303 (1961).
23. V. McLoughlin, R. Moreton, and W. Watt, U.S. Pat. 4,107,408 (1978).
24. V. McLoughlin, R. Moreton, and W. Watt, U.S. Pat. 4,079,122 (1978).
25. M. M. Coleman and G. T. Sivy, *Carbon,* **19,** 123 (1981).
26. G. T. Sivy and M. M. Coleman, *Carbon,* **19,** 127 (1981).
27. M. M. Coleman and G. T. Sivy, *Carbon,* **19,** 133 (1981).
28. G. T. Sivy and M. M. Coleman, *Carbon,* **19,** 137 (1981).
29. G. Henrici-Olivé and S. Olivé, *Polym. Bull.,* **6,** 229 (1982).
30. G. Henrici-Olivé and S. Olivé, *Adv. Polym. Sci.,* **51,** 1–60 (1983).
31. G. T. Sivy, B. Gordon, III, and M. M. Coleman, *Carbon,* **21,** 573 (1983).
32. J.-S. Tsai and C.-H. Lin, *J. Appl. Polym. Sci.,* **43,** 679 (1991).
33. J.-S. Tsai and C.-H. Lin, *J. Appl. Polym. Sci.,* **42,** 3039 (1991).
34. T.-H. Ko, P. Chiranairadul, C.-K, Lu, and C.-H. Lin, *Carbon,* **30,** 647 (1992)
35. W. Watt, D. J. Johnson, and E. Parker, Proc. and Int. Plastic Conf. Carbon Fiber, P3 Plastic Institute, London, 1974.
36. M. Balasubramanian, M. K. Jami, S. K. B. Hattacharya, and A. S. Alhiraman, *J. Mater. Sci.,* **22,** 3864 (1987).
37. H. Marsh and K. Kuo, in *Introduction to carbon Science,* Butterworth & Co., Boston, 1989, p. 130.
38. H. J. Grabke, *Carbon,* **10,** 587 (1972).

*Received June 6, 1995*
*Accepted October 9, 1995*